Int. J. Therm. Sci. (1999) 38, 944–954

Influence of the interfacial free energy crystal/heat transfer surface on the induction period during fouling

Markus Förster, Matthias Bohnet *

Institut für Verfahrens- und Kerntechnik, Langer Kamp 7, 38106 Braunschweig, Germany

(Received 15 January 1999, accepted 26 April 1999)

Abstract — The accumulation of unwanted crystalline deposits (fouling) reduces the efficiency of heat exchangers. In order to adjust the operating conditions with respect to fouling mitigation a model for the description of the entire fouling process has to be established. The main disadvantage of known models is the lack of a description of the induction period which is influenced by the nucleation rate and the adhesive strength between crystals and heat transfer surfaces. The deposition and removal process depends on the interfacial free energy crystal/heat transfer surface. For many industrial applications the only possibility to influence the interfacial free energy is to modify the surface energy characteristics of the heat transfer surface, i.e. its surface free energy. Based on the experimental investigation of the surface energy of several metallic and low energy materials their fouling performance when exposed to a liquid flow of a calcium sulphate solution was evaluated. The deployment of new surface materials such as DLC (diamond like carbon) coatings proved to be a strategy to increase the induction period. © 1999 Éditions scientifiques et médicales Elsevier SAS

fouling / heat transfer surface / crystallisation / nucleation / deposition / removal / induction period / interfacial free energy / new surface materials / adhesion

Résumé — **Influence de l'énergie libre interfaciale cristal / surface de transfert thermique sur la période d'induction de l'encrassement.** La formation de couches cristallines (encrassement) diminue l'efficacité des échangeurs. Afin de fonctionner dans de conditions telles que la formation de couches cristallines soit réduite, il est tout d'abord nécessaire de développer un modèle de calcul de toutes les étapes du processus d'encrassement. L'inconvénient des modèles de calcul connus réside dans le fait qu'ils ne prennent pas en considération la phase d'induction. Cette phase importante dépend de la fréquence de formation des germes et des forces d'adhésion entre la couche cristalline et la surface de l'échangeur. Les deux mécanismes de dépôt et d'érosion dépendent de l'énergie interfaciale entre la couche cristalline et la surface de l'échangeur. Dans de nombreuses applications industrielles, la seule possibilité pour agir sur cette énergie interfaciale consiste à modifier les caractéristiques énergétiques de la surface de l'échangeur, c'est-à-dire son énergie de surface. En nous appuyant sur des études expérimentales concernant l'énergie de surface, nous avons analysé le comportement de la surface de l'échangeur lors d'une expérience d'encrassement avec une solution aqueuse de $CaSO_4$. L'utilisation de nouveaux matériaux de surface, tels que le DLC (*diamond-like carbon*), permet de prolonger la phase d'induction. © 1999 Éditions scientifiques et médicales Elsevier SAS

encrassement / surface d'échangeur / cristallisation / formation de germes / dépôt / érosion / phase d'induction / énergie libre interfaciale / nouveaux matériaux de surface / adhésion

Nomenclature

A	area	m^2
C_i	constant i	
c	concentration	$kg \cdot m^{-3}$
G	Gibbs free energy	J
g	acceleration due to gravity	$m \cdot s^{-2}$
J	rate of nucleation	$m^{-3} \cdot s^{-1}$
k	overall heat transfer coefficient	$W \cdot m^{-2} \cdot K^{-1}$
k_B	Boltzmann constant	$J \cdot K^{-1}$
k_R	rate constant for surface reaction	
$\dot{m}$	mass flow rate per unit area	$kg \cdot m^{-2} \cdot s^{-1}$
n	order of chemical reaction	
p	pressure	Pa
$\dot{Q}$	heat flow	W
R_f	fouling resistance	$m^2 \cdot K \cdot W^{-1}$
r	radius	m
s	thickness	m
T	temperature	K
t	time	h
v	molecular volume	$m^3 \cdot mol^{-1}$
w	flow velocity	$m \cdot s^{-1}$

* Correspondence and reprints.
m.bohnet@tu-bs.de

Greek symbols

β	mass transfer coefficient	$m \cdot s^{-1}$
ϕ	correction factor	
γ_{ij}	interfacial free energy between two adjacent phases i and j	$N \cdot m^{-1}$
η	dynamic viscosity	Pa·s
λ	thermal conductivity	$W \cdot m^{-1} \cdot K^{-1}$
Θ	time constant	s^{-1}
θ	contact angle	deg
ρ	density	$kg \cdot m^{-3}$
σ	shear strength	$N \cdot m^{-2}$
τ	wall shear stress	$N \cdot m^{-2}$
ζ	adhesive strength	$N \cdot m^{-2}$

Superscripts and subscripts

0	clean surface
c	crystalline
crit	critical
d	deposition
dis	dispersive
e	end
F	fluid
f	fouling layer
geo	geometric
het	heterogeneous
hom	homogeneous
ind	induction period
l	liquid
max	maximum
pol	polar
r	removal
S	saturation
s	solid surface
v	volume
w	wall
′	modified

Abbreviations

CCD	charge coupled device
CVD	chemical vapour deposition
DLC	diamond-like carbon
DSA	drop shape analysis
PMMA	polymethylmethacrylate
PTFE	polytetrafluor ethylene

1. INTRODUCTION

The accumulation of crystalline deposits on heat transfer surfaces is usually referred to as fouling. Due to the insulating effect of a fouling layer the presence of these scalings causes a decrease in the overall heat transfer coefficient and, therefore, reduces the efficiency of the heat transfer unit [1]. According to Bott [2], several fouling costs have to be considered when evaluating the additional expenses caused by the decrease of efficiency. First of all increased capital investment, e.g., due to intentional overdimensioning of the heat transfer area in order to make allowance for potential fouling, has to be taken into account. Second, an increase in pressure drop and thermal resistance due to the scaling process leads to additional operating costs. In order to restore the liquid flow and the effectiveness of the heat exchanger frequent cleaning phases have to be carried out. This leads to increased costs due to the loss of production and remedial action. These parts of the overall fouling cost represent just an selection of all possible expenses caused by precipitation fouling. In a very intensive study Garret-Price et al. [3] estimate the annual cost of fouling and corrosion for the US industry to be $3–10 billion. This cost estimation emphasises the need to face the problem of fouling. Favourable operating conditions in order to mitigate fouling can only be chosen based on an appropriate physical model. The establishment of such a model describing both the induction and fouling period (*figure 1*) is one of the major objectives of fouling research work. The decrease of efficiency due to scale formation can be characterised by means of the fouling resistance R_f defined by the equation

$$R_f = \frac{1}{k_f} - \frac{1}{k_0} \tag{1}$$

where k_f is the overall heat transfer coefficient for the fouled and k_0 for the clean heat transfer surface.

Figure 1 shows the measured fouling resistance R_f versus time for a typical test. During the fouling process

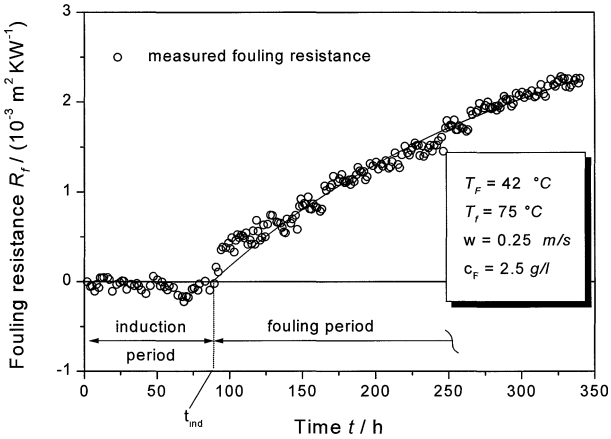

Figure 1. Fouling resistance versus time for an aqueous $CaSO_4$ solution as the liquid phase (surface material: stainless steel).

two periods of time can be identified. In the first period the formation of stable crystalline nuclei and their concretion to a compact fouling layer take place. This period is called the "induction period". In the succeeding "fouling period" a decrease of the overall heat transfer coefficient due to scale formation can be measured. Recent approaches to describe the entire fouling process mainly concentrate on the investigation of the fouling period (e.g., [4–6]). The important induction period t_{ind} is quite often neglected, although this period represents a remarkable potential to mitigate fouling.

2. FOULING PERIOD

During the fouling period both the deposition and the removal process have to be taken into account (*figure 2*). The relationship between these two processes and the fouling resistance R_{f} is given by

$$\frac{\mathrm{d}R_{\mathrm{f}}}{\mathrm{d}t} = \frac{1}{\lambda_{\mathrm{f}}\rho_{\mathrm{f}}}\left(\dot{m}_{\mathrm{d}} - \dot{m}_{\mathrm{r}}\right) \tag{2}$$

where λ_{f} is the thermal conductivity and ρ_{f} the density of the fouling layer. $\dot{m}_{\mathrm{d}}$ and $\dot{m}_{\mathrm{r}}$ are the mass deposition and removal rates.

2.1. Deposition process

Berthoud [7] and Valeton [8] assume that the deposition process characterised by the mass deposition rate $\dot{m}_{\mathrm{d}}$ consists of two stages. A diffusion process of the salt ions to the solid is followed by a chemical reaction in the adsorption layer when the ions arrange themselves into the crystal lattice. The equations to describe these two stages may be written as

$$\dot{m}_{\mathrm{d}} = \beta(c_{\mathrm{F}} - c_{\mathrm{f}}) \quad \text{(diffusion)} \tag{3}$$

$$\dot{m}_{\mathrm{d}} = \frac{A_{\mathrm{real}}}{A_{\mathrm{geo}}}\, k_{\mathrm{R}}(c_{\mathrm{f}} - c_{\mathrm{S}})^n = k'_{\mathrm{R}}(c_{\mathrm{f}} - c_{\mathrm{S}})^n \quad \text{(chemical reaction)} \tag{4}$$

where β is the mass transfer coefficient and k_{R} the rate constant for the surface reaction. According to *figure 2*, c_{F} and c_{f} are the concentrations in the bulk and at the transition to the adsorption layer, respectively, whereas c_{S} is the saturation concentration. Hirsch [9] introduced a geometric correction factor $A_{\mathrm{real}}/A_{\mathrm{geo}}$, since the real surface of a fouling layer is always larger than the corresponding geometric surface. The average value of the correction factor was derived from numerous experiments, i.e.

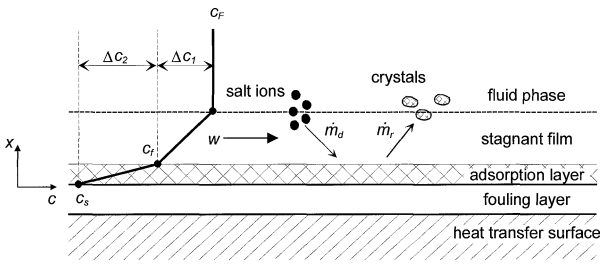

Figure 2. Deposition and removal during the fouling period.

$A_{\mathrm{real}}/A_{\mathrm{geo}} = 1.95$. The assumption of a second order chemical reaction with $n = 2$ leads to satisfactory results in describing reality. Combining equations (3) and (4) gives:

$$\dot{m}_{\mathrm{d}} = \beta\left[\frac{1}{2}\left(\frac{\beta}{k'_{\mathrm{R}}}\right) + (c_{\mathrm{F}} - c_{\mathrm{S}}) - \sqrt{\frac{1}{4}\left(\frac{\beta}{k'_{\mathrm{R}}}\right)^2 + \left(\frac{\beta}{k'_{\mathrm{R}}}\right)(c_{\mathrm{F}} - c_{\mathrm{S}})}\right] \tag{5}$$

2.2. Removal process

The fouling layer on the heat transfer surface is exposed to a wall shear stress τ due to the liquid flow. For the characterisation of the removal process, Bohnet [10] suggests:

$$\dot{m}_{\mathrm{r}} = C_1\left(\frac{\eta g}{\rho}\right)^{1/3}\frac{\rho_{\mathrm{f}}}{\sigma_{\mathrm{f}}}\tau \tag{6}$$

where η is the viscosity and ρ the density of the fluid phase. The ratio of the density to the shear strength of the deposit $\rho_{\mathrm{f}}/\sigma_{\mathrm{f}}$ is a function of the thickness of the fouling layer. Hirsch [9] identified the constant, $C_1 = 2.75 \cdot 10^{-3}$. Furthermore, he provided an equation to substitute the unknown expression $\rho_{\mathrm{f}}/\sigma_{\mathrm{f}}$ in equation (6) by

$$\frac{\rho_{\mathrm{f}}}{\sigma_{\mathrm{f}}} = \frac{\mathrm{d}(\rho_{\mathrm{f}}/\sigma_{\mathrm{f}})}{\mathrm{d}x_{\mathrm{f}}}x_{\mathrm{f}} \tag{7}$$

The shear gradient

$$\frac{\mathrm{d}(\rho_{\mathrm{f}}/\sigma_{\mathrm{f}})}{\mathrm{d}x_{\mathrm{f}}}$$

depends on the operating conditions of the heat exchanger.

Using equations (5) and (6) and the relationship between mass per unit area m_{f} and fouling resistance:

$$m_{\mathrm{f}} = \rho_{\mathrm{f}}x_{\mathrm{f}} = \rho_{\mathrm{f}}\lambda_{\mathrm{f}}R_{\mathrm{f}} \tag{8}$$

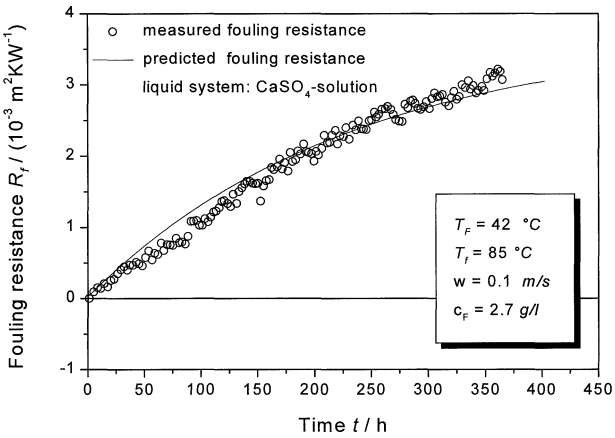

Figure 3. Comparison of measured and predicted fouling resistance as a function of time.

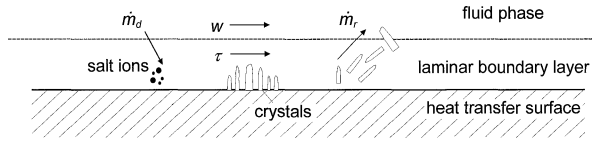

Figure 4. Deposition and removal during the induction period.

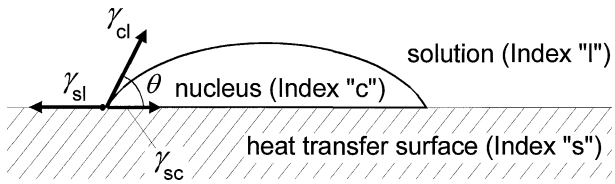

Figure 5. Interfacial free energies at the boundaries between three phases.

equation (2) can be rearranged to give the following form:

$$\frac{\mathrm{d}R_\mathrm{f}}{\mathrm{d}t} = \frac{1}{\rho_\mathrm{f}\lambda_\mathrm{f}}\left[\dot{m}_\mathrm{d} - C_1\left(\frac{\eta g}{\rho}\right)^{1/3}\frac{\mathrm{d}(\rho_\mathrm{f}/\sigma_\mathrm{f})}{\mathrm{d}x_\mathrm{f}}\tau\lambda_\mathrm{f}R_\mathrm{f}\right] \quad (9)$$

Integrating equation (9) yields the model equation to describe the fouling period:

$$R_\mathrm{f} = R_\mathrm{f}^*\left[1 - \mathrm{e}^{-\Theta(t-t_\mathrm{ind})}\right] \quad (10)$$

with

$$R_\mathrm{f}^* = \frac{\dot{m}_\mathrm{d}}{C_1(\eta g/\rho)^{1/3}(\mathrm{d}(\rho_\mathrm{f}/\sigma_\mathrm{f})/\mathrm{d}x_\mathrm{f})\tau\lambda_\mathrm{f}} \quad (11)$$

and

$$\Theta = C_1\left(\frac{\eta g}{\rho}\right)^{1/3}\frac{\mathrm{d}(\rho_\mathrm{f}/\sigma_\mathrm{f})}{\mathrm{d}x_\mathrm{f}}\frac{\tau}{\rho_\mathrm{f}} \quad (12)$$

In *figure 3*, the measured fouling resistance for a $CaSO_4$ solution is compared to predicted data derived by means of the model equation. It can be seen that the predicted fouling resistance is in good agreement with reality.

3. INDUCTION PERIOD

Since appropriate models to describe the fouling period are already available, one of the main objectives of fouling research work is the detailed investigation of the induction period in order to define a model able to describe the entire fouling process. For industrial applications the duration of t_ind should be as long as possible. Similar to the fouling period the induction period also consists of a deposition and a removal process (*figure 4*).

The induction period is mainly influenced by free interfacial energies. Since the interfacial zone of two bulk phases in contact is non-homogeneous, a pressure gradient perpendicular to the interfacial boundary is observed. The pressure in a bulk phase is homogeneous and isotropic. Therefore, no net energy is expended in reversibly transporting matter within a bulk phase. On the other hand, a net energy is required to create an interface by transporting the matter from the bulk phase to the interfacial region [11]. The reversible work to create an unit interfacial surface area is the interfacial free energy, that is:

$$\gamma_{ij} = \left(\frac{\partial G}{\partial A}\right)_{T,p} \quad (13)$$

where γ_{ij} is the interfacial free energy at the interface of the phases i and j, G the Gibbs free energy of the total system, A the interfacial area, T the temperature and p the pressure. Considering fluid/fluid interfaces the interfacial free energy and the interfacial tension are equal. Analogous to wetting theories *figure 5* shows a nucleus crystallised on a solid heat transfer surface during the initiation stage of the fouling process. In this case the three phases are two solids (heat transfer surface and crystal) and a liquid (salt solution) [12].

Figure 5 represents the thermodynamic equilibrium by means of the angle of contact θ between the crystalline deposit and the solid heat transfer surface. This contact angle corresponds to the angle of wetting in liquid/solid/vapour systems. The three interfacial free energies are denoted γ_sl (between heat transfer surface s and liquid solution l), γ_sc (between heat transfer surface and crystal nucleus c) and γ_cl (between crystal nucleus and liquid solution). Resolving the interfacial free energies in

a horizontal direction leads to the Young equation:

$$\gamma_{sl} = \gamma_{sc} + \gamma_{cl} \cos\theta \tag{14}$$

3.1. Deposition process

The homogeneous nucleation without regard for the heat transfer surface is characterised by the overall excess free energy ΔG^{hom} of the system. Mullin [13] presents a detailed description of both homogeneous and heterogeneous nucleation. Under certain circumstances ΔG^{hom} only consists of a negative component ΔG_v, i.e. the excess free energy which is released when the formation of the volume of the new crystalline phase takes place, and of a positive component ΔG_s, i.e. the excess free energy which is absorbed for the generation of the new interface. The sum of both components ΔG_v and ΔG_s leads to ΔG^{hom} as a function of the size of the nucleus r (*figure 6*).

$\Delta G^{hom}(r)$ passes through a critical maximum ΔG^{hom}_{crit} corresponding to the critical nucleus size r_{crit}. The formation of critical nuclei is favoured since ΔG^{hom}_{crit} corresponds to a maximum energy decrease. The relationship

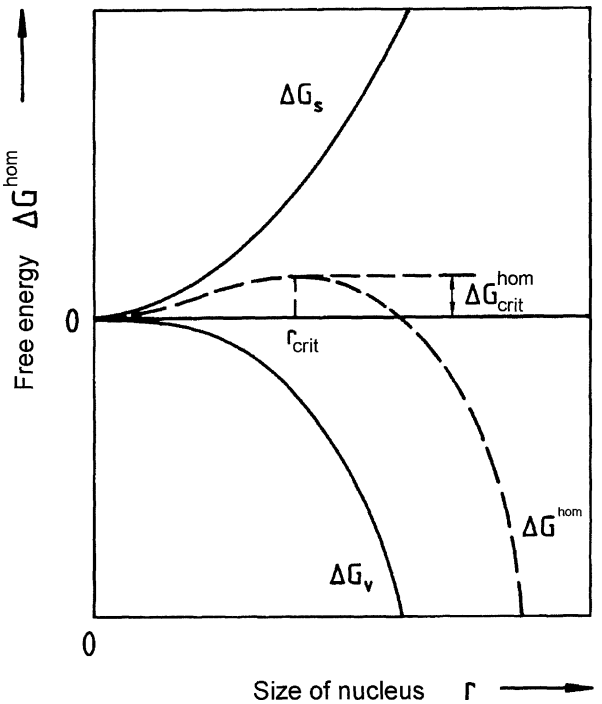

Figure 6. Free energy diagram for homogeneous nucleation [12].

between ΔG^{hom}_{crit} and r_{crit} can be written as

$$\Delta G^{hom}_{crit} = \frac{4}{3}\pi\gamma_{cl} r^2_{crit} = \frac{16}{3}\pi \frac{\gamma^2_{cl} v^2}{[k_B T \ln(c/c_S)]^2} \tag{15}$$

where k_B is the Boltzmann constant and v is the molecular volume. As the presence of a heat transfer surface favours nucleation the critical excess free energy ΔG^{hom}_{crit} is larger than ΔG^{het}_{crit}, the corresponding excess free energy associated with heterogeneous nucleation. Thus,

$$\Delta G^{het}_{crit} = \phi \Delta G^{hom}_{crit} \tag{16}$$

where the correction factor ϕ is less than unity. Volmer [14] provides an equation to calculate ϕ, i.e.

$$\phi = \frac{(2 + \cos\theta)(1 - \cos\theta)^2}{4} \tag{17}$$

Based on the Arrhenius reaction velocity equation the relationship between the critical number of nuclei formed per unit time and unit volume J^{het} (rate of nucleation) can be written:

$$J^{het} = C_2 \exp\left(-\frac{\Delta G^{het}_{crit}}{k_B T}\right) \tag{18}$$

Under certain circumstances the rate of nucleation J^{het} is directly proportional to the mass deposition rate $\dot{m}_d$ within the induction period. Hence, the use of equations (15)–(18) leads to

$$\dot{m}_d = C_3 \exp\left[-\phi \frac{16\pi}{3} \frac{\gamma^3_{cl} v^2}{k^3_B T^3 \ln^2(c/c_S)}\right] \tag{19}$$

Equation (19) provides a relationship between the mass deposition rate $\dot{m}_d$ and the correction factor ϕ. According to equation (17) this factor is a function of the equilibrium contact angle θ only. Using the Young equation (14) it is obvious that the variation of the interfacial free energy γ_{sl} is one way to modify $\dot{m}_d$ since γ_{cl} is fixed (for a given liquid system) and both γ_{sc} and θ result from the thermodynamic equilibrium. Therefore, for given operating conditions and physical properties of the liquid, one way to mitigate precipitation fouling during the induction period is to modify the surface characteristics, e.g., the energy related properties of the heat transfer surface. Because the interfacial free energy γ_{sl} is directly influenced by the surface free energy γ_{sv} of the heat transfer surface the choice of the surface material has a crucial effect on the deposition process.

3.2. Removal process

The crystals growing on the heat transfer surface are exposed to the wall shear stress τ caused by the liquid flow:

$$\tau = C_4 \rho w^2 \tag{20}$$

The wall shear stress interacts with the adhesive strength ζ between the crystalline deposit and the heat transfer surface. For optimisation of the efficiency of heat transfer units ζ has to be minimized. Dyckerhoff [15] explored the dependence of the surface free energy γ_{sv} of the substrate on the adhesion substrate/adhesive. According to *figure 7*, the adhesive strength between a lacquer and polyurethane has been measured.

The two surface free energies are denoted γ_{sv} (of the polymer used as substrate) and γ_{lv} (of the hardened lacquer used as adhesive). According to *figure 7*, the adhesive strength ζ has a maximum when the surface free energy of the adhesive is equal to that of the substrate, i.e. when the interfacial energy adhesive/substrate has a minimum. This fact stands in contradiction to the thesis that improving wettability by means of increasing γ_{sv} always increases ζ. Transferring these facts to the fouling phenomenon leads to the conclusion that the surface free energy of the heat transfer surface has to become a minimum taking also the nucleation rate associated with the deposition process into consideration which decreases when using low-energy surfaces. For the investigation of low energy surfaces see also [16].

Since the surface free energy γ_{sv} has a crucial influence on both the deposition and removal process, the surface energy characteristics of several surface materials and their performance in real fouling test runs have been examined.

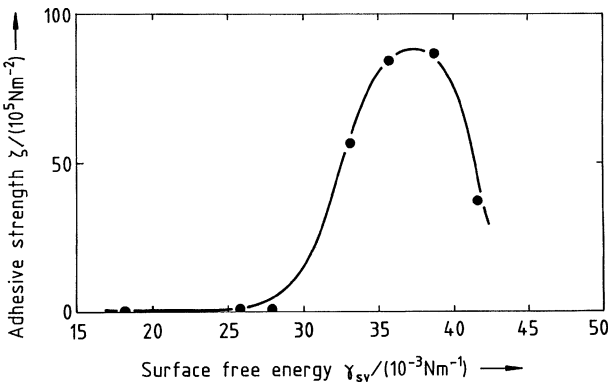

Figure 7. Adhesive strength polyurethane/lacquer (γ_{lv} = 37.5 mN·m^{-1}) versus surface free energy of the substrate [15].

4. EXAMINATION OF SURFACE CHARACTERISTICS

The surface free energy γ_{sv} of the heat transfer surface is examined by wetting experiments. The method uses droplets of several test liquids resting on the surface. After the contact angle has been measured γ_{sv} of the solid substrate can be calculated. θ can been determined with a DSA (drop shape analysis) measurement device. The arrangement of the optical measurement device is given in *figure 8*.

The image of the droplet resting on the solid substrate is digitised by means of a CCD-camera and a data processing system. A commercial program helps to measure the dynamic contact angle θ and to evaluate the surface free energy γ_{sv}. In order to calculate γ_{sv} the Young equation (14) can be employed:

$$\gamma_{sv} = \gamma_{sl} + \gamma_{lv} \cos\theta \tag{21}$$

where now the interfacial energies of the phase boundaries in contact correspond to a solid (index "s"), liquid (index "l") and vapour (index "v") system. According to Fowkes [17], the total interfacial free energy of the interface between two bulk phases i and j can be subdivided into a fluctuating dispersive component γ_{ij}^{dis} and a permanent polar component γ_{ij}^{pol}. Assuming that the physical properties of the liquids, i.e. γ_{lv}^{pol} and γ_{lv}^{dis}, are accessible, the only unknown parameter to determine γ_{sv}^{pol} and γ_{sv}^{dis}, after having measured the contact angle, is the interfacial free energy between solid substrate and liquid droplet γ_{sl}. The *table I* shows three different approaches to describe γ_{sl}.

The geometric-mean method according to equation (22) is frequently used to substitute γ_{sl} in the Young equation (21). Rearranging the latter equation a linear relationship between a x- and y-value can be derived, de-

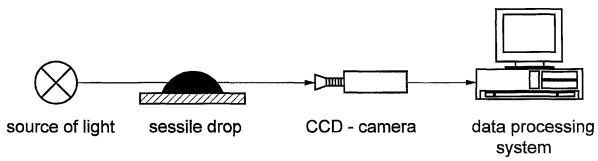

Figure 8. Experimental arrangement of the DSA measurement device.

TABLE I
Methods for calculating the interfacial free energy γ_{sl} [11].

γ_{sl}	Field of application	Equation
$\gamma_{sv}+\gamma_{lv}-2\left(\sqrt{\gamma_{sv}^{dis}\gamma_{lv}^{dis}}+\sqrt{\gamma_{sv}^{pol}\gamma_{lv}^{pol}}\right)$	geometric-mean method for non-polar surfaces	(22)
$\gamma_{sv}+\gamma_{lv}-4\left(\frac{\gamma_{sv}^{dis}\gamma_{lv}^{dis}}{\gamma_{sv}^{dis}+\gamma_{lv}^{dis}}+\frac{\gamma_{sv}^{pol}\gamma_{lv}^{pol}}{\gamma_{sv}^{pol}+\gamma_{lv}^{pol}}\right)$	harmonic-mean method for low-energy surfaces	(23)
$\gamma_{sv}+\gamma_{lv}-2\sqrt{\gamma_{sv}^{dis}\gamma_{lv}^{dis}}-4\frac{\gamma_{sv}^{pol}\gamma_{lv}^{pol}}{\gamma_{sv}^{pol}+\gamma_{lv}^{pol}}$	geometric–harmonic-mean method for high-energy surfaces	(24)

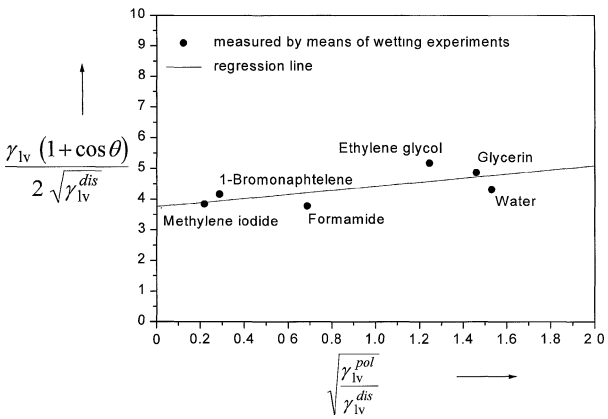

Figure 9. Regression analysis for the determination of the surface energy characteristics of a PTFE-coated heat transfer surface.

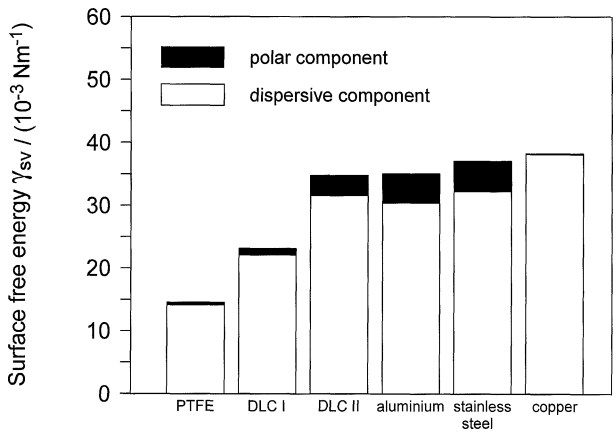

Figure 10. Surface free energies of several surface materials.

pending on the known physical properties of the test liquid and the measured contact angle:

$$\underbrace{\frac{\gamma_{lv}(1+\cos\theta)}{2\sqrt{\gamma_{lv}^{dis}}}}_{y}=\sqrt{\gamma_{sv}^{dis}}+\sqrt{\gamma_{sv}^{pol}}\underbrace{\sqrt{\frac{\gamma_{lv}^{pol}}{\gamma_{lv}^{dis}}}}_{x} \qquad (25)$$

Each test liquid used in a wetting experiment yields one data point in a diagram according to *figure 9*. Based on a linear regression the polar and dispersive components of γ_{sv} of the heat transfer surface can be determined. The accuracy of this graphical method is improved with an increasing amount of test liquids. In *figure 9* six test liquids have been used to examine the energy related surface properties of a steel heat transfer surface coated with PTFE (polytetrafluorethylene).

The regression analysis gives $\gamma_{sv}^{pol}=0.44$ mN·m^{-1} and $\gamma_{sv}^{dis}=14.12$ mN·m^{-1}. The sum of these two components leads to the total surface free energy of the heat transfer surface $\gamma_{sv}=14.56$ mN·m^{-1}. Applying the geometric-mean method [equation (22)] to evaluate the energy, characteristics of heat transfer surfaces results, according to *figure 10*, are obtained. In this diagram DLC stands for diamond-like carbon coatings produced in a chemical vapour deposition (CVD) process, DLC I and DLC II for special modifications of their structural constitution. The DLC-coatings have been developed and produced by the Fraunhofer Institute for Thin Films and Surface Engineering (Braunschweig, Germany), see also [18, 19].

As previously mentioned, the deposition process of the induction period is favoured when γ_{sv} of the heat transfer surface is reduced by the choice of appropriate surface materials. Since PTFE has the lowest value of surface free energy, a long induction period can be expected.

On the other hand, several disadvantages of this low-energy surface material have to be taken into account. In order to meet wear requirements polymer coatings must have a minimum layer thickness. This implies a reduced efficiency due to the low coefficient of thermal conductivity of PTFE. Another crucial disadvantage is the low temperature stability of polymers (PTFE: $T_{max} \approx 525$ K). An interesting alternative is the deployment of DLC-coatings. Better abrasion characteristics and temperature stability of these new surfaces compared to polymers while still a low surface energy can be realised have to be opposed to increased production cost. Besides the examination of the energy related characteristics of the interesting heat transfer surfaces, the adhesion phenomenon has to be explored in order to receive information on the removal process within induction period. Deposits of calcium sulphate are produced upon substrates to be characterised. With the help of a ring shear device the adhesive strength between the test cylinders and the solid substrates can be determined. In *figure 11* test results of adhesive strength measurements with two water–gypsum ratios (WGR) for particular substrate materials are presented.

By means of a surface texture measuring unit it was confirmed that the surface topographies of the surfaces discussed above resemble each other. Hence, the influence of surface texture could be eliminated for analysis of the experimental results given in *figure 11*. Since the average adhesive strength between $CaSO_4$ deposits and heat transfer surfaces coated with DLC is much lower than the corresponding average value for metallic surfaces, a significantly longer induction period for heat transfer surfaces treated in a CVD process can be expected.

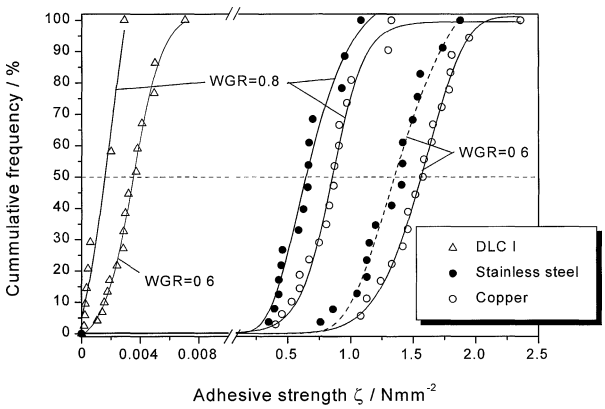

Figure 11. Frequency distribution curves of the adhesive strength between crystalline deposits ($CaSO_4$) and particular solids.

5. FOULING EXPERIMENTS

Figure 12 is a schematic diagram of the experimental unit used for fouling experiments.

The filter avoids sedimentation of particles and secondary nucleation in the test sections since seed particles can influence nucleation behaviour considerably. The heat exchanger guarantees a constant inlet temperature to the test sections. The first and second test section consist of annular test tubes used for reference measurements. The third test section includes a plate heat exchanger suited for easy replacement of its heat transfer surface when different materials have to be analysed with respect to their fouling performance. According to *figure 13* the surface is heated by three rod heaters. The temperature of the test surface is measured using six thermocouples in order to determine the fouling resistance. The wall of the test section contains a transparent section made of PMMA for the observation of the fouling process, especially of the induction period. This helps to identify regions where preferential nucleation occurs.

Figure 14 provides the fouling resistance versus time as a function of the temperature for a heat transfer surface made of stainless steel. It is obvious that the duration of the induction period is increased by low wall temperatures T_w since the nucleation process using salt solutions of inverse solubility is favoured by high temperatures. For the fouling experiments the initial wall temperature is $T_w = 75\,°C$. An increase of flow velocity corresponds to higher shear forces acting on the crystals

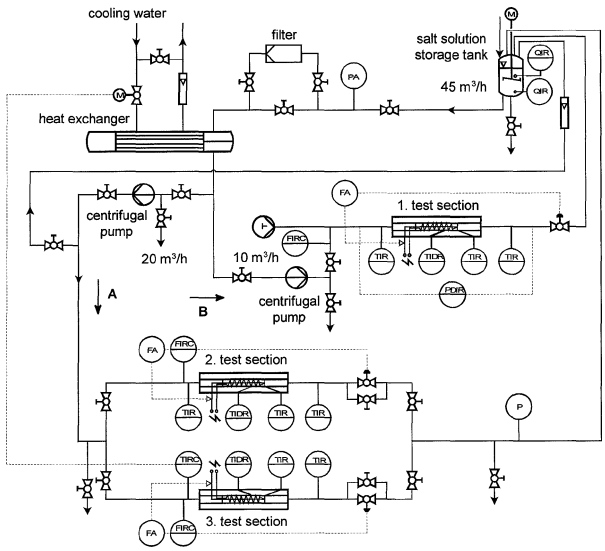

Figure 12. Flow sheet of the experimental unit.

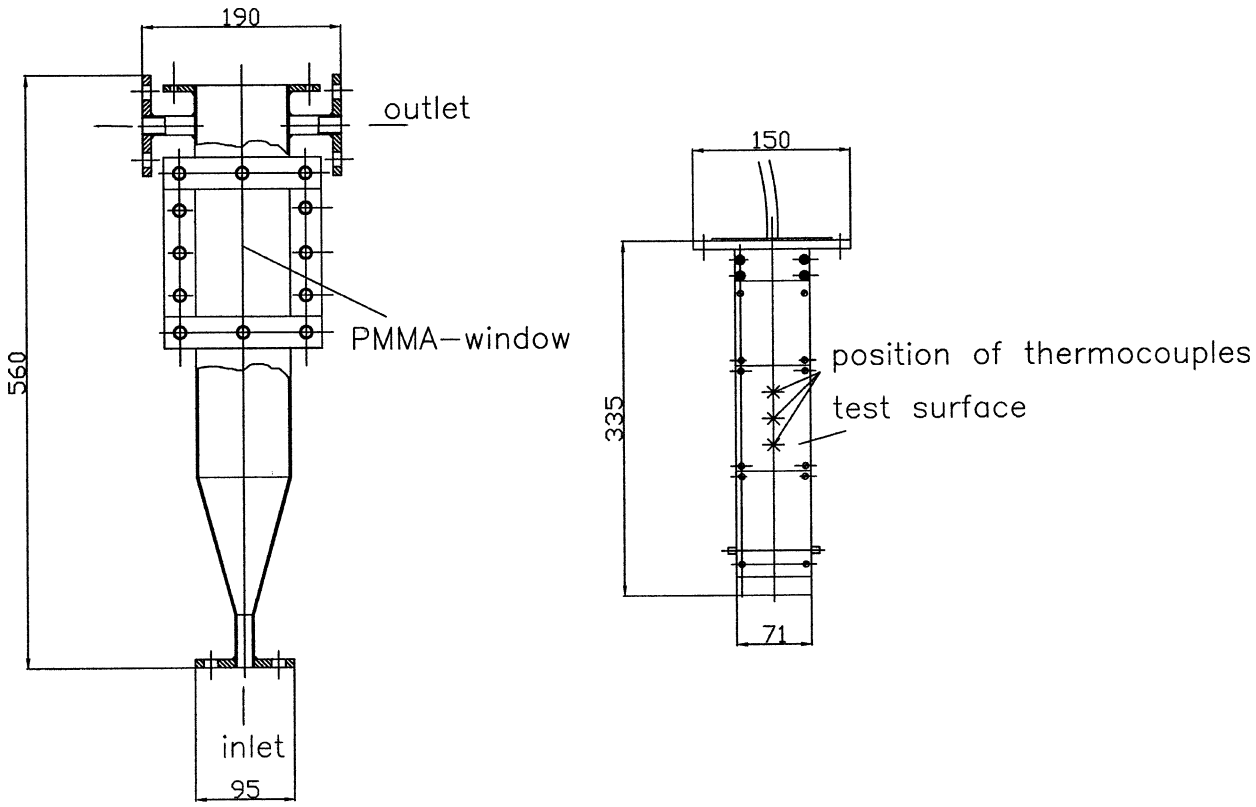

Figure 13. Plate heat exchanger.

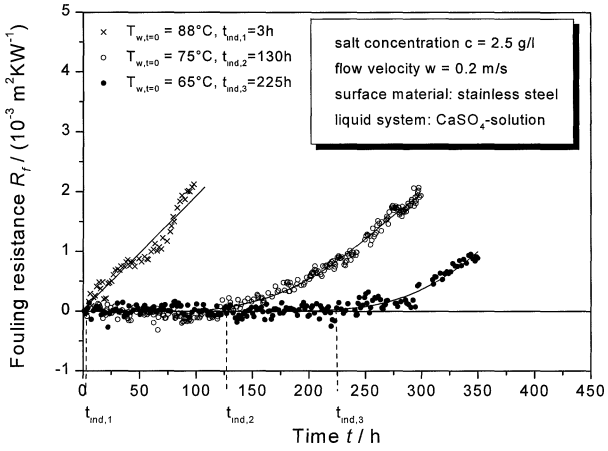

Figure 14. Influence of the operating conditions on the induction period.

resulting in an increase of induction time. In order to avoid a long duration of fouling experiments the flow velocity has been fixed to $w = 0.2$ m·s^{-1}, giving an induction period of $t_{ind} = 130$ h for a test surface made of stainless steel. All experiments have been performed using an aqueous calcium sulphate solution.

Figure 15 shows results of fouling test runs for several metallic surfaces. The induction period for a surface made of copper ($t_{ind,1} = 30.5$ h) is lower than for a surface made of stainless steel ($t_{ind,3} = 130$ h) since the average adhesive strength between crystals of calcium sulphate and the stainless steel surface is always lower than the corresponding value for a copper surface (*figure 11*). According to *figure 10*, copper has the largest surface free energy γ_{sv} of all materials which have been examined. This fact favours both the rate of nucleation and the adhesive strength crystal/heat exchanger surface. Once a compact crystalline deposit has formed on the heat transfer surface the influence of surface material decreases. The fouling curve derived when inserting a test surface made of aluminium gives an induction period ($t_{ind,2} = 48$ h) lower than a steel surface despite its lower surface free energy according to *figure 10*. This can be explained when examining the aluminium surface after exposition to the liquid flow of a calcium sulphate solution. The corrosion of this metallic surface,

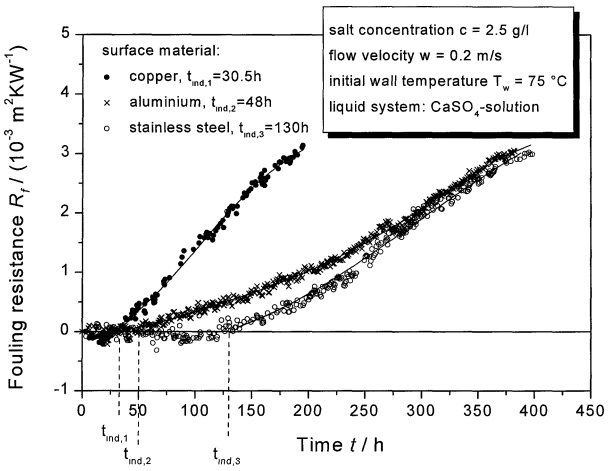

Figure 15. Fouling resistance versus time for metallic heat transfer surfaces.

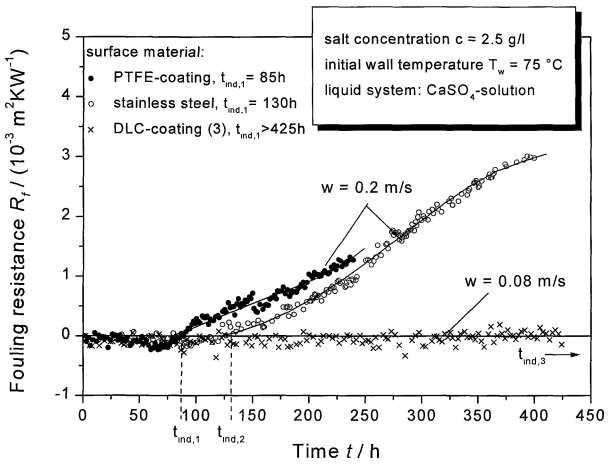

Figure 16. Fouling resistance versus time for low energy heat transfer surfaces.

i.e. the deterioration and loss of surface material due to a chemical surface reaction, implies a variation of surface energy.

In *figure 16* the results of the measured fouling resistance as a function of time for low-energy surfaces are accumulated. The fouling curve for the stainless steel surface is added for comparison. The deployment of a polymer surface coating demands a minimal thickness of the coating (here: 20 μm) because the thermal resistance of the organic film is high. The requirement of a minimal layer thickness results in an inhomogeneous texture of the surface coating due to the production process causing regions for preferential nucleation. Once a fouling layer has grown on the polymer surface under a constant heat flux, the PTFE material is destroyed because of the temperature increase at the interface coating/scaling. Thus, it can be concluded that low-energy surfaces made of a polymer are not well suited for heat exchangers exposed to liquid salt solutions of inverse solubility, at least for the geometric boundary constraints and operating conditions that have been examined. In contrast, the insertion of DLC surface materials in the test section results in an induction period that is much more significant. In spite of decreasing the flow velocity to 40 % of the corresponding value for the polymer and metallic surfaces (τ decreases considerably), no increase in the thermal resistance due to crystalline deposits can be measured after a test run of more than 425 h. This indicates that the system is still within the induction period.

Figure 17. Heating element (surface material: stainless steel), $t_e = 450$ h.

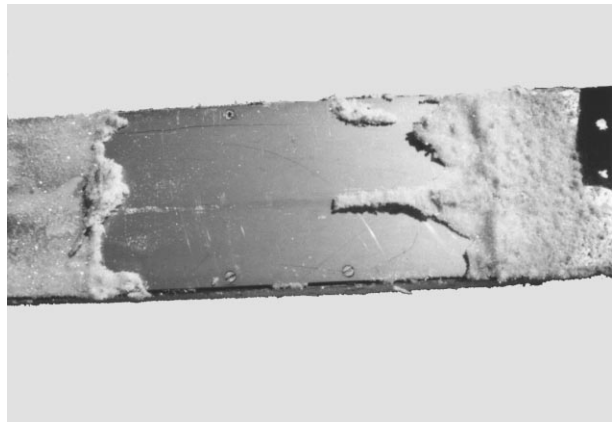

Figure 18. Heating element (surface material: DLC-coating), $t_e = 450$ h.

Figure 17 shows the uncoated heating element after a 450 h-test run (surface material: stainless steel). On the test surface a fouling layer of a thickness of several

millimetres can be observed. *Figure 18* represents the surface conditions for the DLC-coated steel surface. After 450 h, no crystalline clusters can be detected on the low-energy surface.

6. CONCLUSIONS AND FUTURE WORK

The lack of an appropriate model to describe the induction period of the fouling process on heat transfer surfaces motivates the exploration of deposition and removal mechanisms. Both mechanisms are influenced by the surface free energy of the solid heat transfer surface. Since the duration of the induction period decreases with high-energy surfaces, the main interest concerning industrial applications is to produce low-energy surfaces. This would help to reduce both the nucleation rate and adhesive strength between crystals and the particular heat transfer surface. Hence, the duration of the induction period could be increased resulting in reduced fouling cost. Since the application of low-energy polymer coatings on common heat transfer surface materials has several disadvantages, the deployment of low-energy DLC-coatings produced in a chemical vapour deposition process is an interesting alternative. With the help of an experimental unit it has been shown on the basis of test runs with a calcium sulphate solution that the use of such DLC-coatings results in a significantly long induction period. For the prediction of the initiation stage of the fouling process the energy-related surface characteristics of the corresponding surface materials have to be determined. Future work should concentrate on the establishment of an appropriate model to describe both the induction and fouling period. Besides the energy-related properties of the heat transfer surface, its geometric features can also influence the deposition and removal mechanism of the induction period since smoothing effects of the original surface texture of the corresponding substrate when using thin coatings could also result in an increased length of the induction period. Thus, the effect of surface texture on the induction period has to be taken into account when a model is developed.

Acknowledgement

Financial support for this research work has been granted by the DFG (Deutsche Forschungsgemeinschaft).

REFERENCES

[1] Krause S., Fouling an Wärmeübertragungsflächen durch Kristallisation und Sedimentation, VDI-Forschungsheft 637 (1986) 1–44.

[2] Bott T.R., Fouling of Heat Exchangers, Elsevier Science, Amsterdam, 1994.

[3] Garret-Price B.A., Smith S.A., Watts R.L., Knudsen J.G., Marner W.J., Suitor J.W., Fouling of Heat Exchangers. Characteristics, Costs, Prevention, Control and Removal, Noyes Publications, Park Ridge, NJ, 1985.

[4] Bohnet M., Augustin W., Middis J., Effect of surface structure on fouling behaviour, in: Proc. Eurotherm Seminar 23, Grenoble, 1992, pp. 39–46.

[5] Augustin W., Bohnet M., Influence of the ratio of free hydrogen ions on crystallisation fouling, Chem. Engrg. Proc. 34 (1995) 79–85.

[6] Hirsch H., Augustin W., Bohnet M., Über den Abtrag von Kristallschichten an wärmeübertragenden Flächen, Chem. Ing. Tech. 68 (1996) 691–694.

[7] Berthoud A., Théorie de la formation des faces d'un cristal, J. Chim. Phys. 10 (1912) 624–635.

[8] Valeton J.J.P., Wachstum und Auflösung der Kristalle, Zeitschrift für Kristallographie 59 (1924) 483.

[9] Hirsch H., Scher- und Haftfestigkeit kristalliner Foulingschichten auf wärmeübertragenden Flächen, Shaker Verlag, Aachen, 1997.

[10] Bohnet M., Fouling of heat transfer surfaces, Chem. Engrg. Technol. 10 (1987) 113–125.

[11] Wu S., Polymer Interface and Adhesion, Marcel Dekker Inc., New York, 1982.

[12] Matz G., Kristallisation, Springer-Verlag, Berlin, Heidelberg, 1969.

[13] Mullin J.W., Crystallization, Butterworth-Heinemann, Oxford, 1993.

[14] Volmer M., Kinetik der Phasenbildung, Steinkopf, Leipzig, 1939.

[15] Dyckerhoff G.A., Über den Einfluß der Grenzflächenergie auf die Haftfestigkeit, Angew. Makromol. Chem. 21 (1972) 169–185.

[16] Müller-Steinhagen H., Zhao Q., Investigation of low fouling surface alloys made by ion implantation technology, Chem. Engrg. Sci. 52 (1997) 3321–3332.

[17] Fowkes F.M. Dispersion force contribution to surface and interfacial tensions, contact angles and heats of immersion, in: Adv. Chem. Ser., Vol. 43 (1964) pp. 99–111.

[18] Grischke M., Entwicklung eines Strukturmodells metallhaltiger Kohlenwasserstoff-Schichten [a-C:H(Me)] mit carbidbildender Metallkomponente, VDI-Verlag, Düsseldorf, 1989.

[19] Trojan K., Untersuchungen zum Einfluß netzwerkmodifizierender Elemente auf die freie Oberflächenenergie amorpher Kohlenwasserstoff-Schichten, VDI-Verlag, Düsseldorf, 1996.